H.M. Kolkovska[1], B.I. Rachiy[1], P.I. Kolkovskyi[1], I.P. Yaremiy[1],
N.Ya. Ivanichok[1], R.P. Lisovskiy[2], N.R. Ilnytskyi[2]

Mechanisms of Charge Accumulation of the Electrochemical System LaMnO₃ / AC

[1]*Vasyl Stefanyk Precarpathian National University, Ivano-Frankivsk, Ukraine, e-mail: Pkolkovskyy@gmail.com*
[2]*Ivano-Frankivsk National Medical University, Ivano-Frankivsk, Ukraine, Rlisovsky@ifnmu.edu.ua*

In this work, the electrochemical behavior of LaMnO₃ perovskite material and nanoporous carbon material in an aqueous solution of lithium sulfate are studied. The regularities of the expediency of the joint functioning of these materials as electrodes for a hybrid electrochemical capacitor are determined. It was found that the value of the specific capacity of the investigated electrochemical system of LaMnO₃ / electrolyte / AC is 52 F/g during the discharge of the system to 1 V and the value of specific energy is 112.1 J/g at a discharge current of 1 mA.

Keywords: LaMnO₃ manganite, activated carbon, Li₂SO₄ electrolyte, specific capacity.

Introduction

Electrochemical capacitors (EC) are one of the most promising electrical energy storage devices. Thus, ECs fill the gap between batteries and conventional capacitors, demonstrating a relatively high specific energy and power, as well as the ability to operate at a significant number of charge/discharge cycles [1]. However, there are certain disadvantages associated with the limitation on the increase of the specific energy of EC. These limitations are the main impetus for the implementation of non-standard solutions to problems related to the values of battery parameters, in particular the relatively small number of charge / discharge cycles and insufficiently high specific power and specific energy. One of the non-standard solutions is the concept of a hybrid electrochemical capacitor (HEC), which is a mixed battery-capacitor electrochemical system [2]. HEC is characterized by two mechanisms of charge accumulation: the Faraday process and the double electric layer (DEL). The first mechanism is carried out due to the redox reaction on the electrode surface by the ionic intercalation / deintercalation process [3]. The second mechanism is characterized by the formation of a double electric layer at the interface between the electrode material and the electrolyte [4]. Increasing the capacity and stability of the charge-discharge cycle are the main reasons for finding new electrode materials for both EC and HEC [5].

Recently, as electrode materials for electrochemical capacitors, much attention is paid to materials with a perovskite structure. Perovskite materials have the chemical formula ABO₃, where position A is occupied by a rare earth ion, such as lanthanum (La), neodymium (Nd), and position B is occupied by transition metal ions with 6-fold coordination. If position B is occupied by manganese ions, then such compounds are called manganites [6, 7]. A feature of the perovskite structure is its ability to possible combinations with fragments of other structures, as a result of which new frame or layered composite structures may appear and their characteristics can be significantly improved [8]. Materials of this type are also widely studied as functional materials of electronic technology, laser materials, sensors, catalysts [9], and materials for solar cells [10]. The resistance of these materials to high temperatures allows them to be used as electrode materials in energy storage and conversion devices [11-14]. Among the most widely used perovskite materials,

much attention is paid to lanthanum manganite (LaMnO$_3$), which is characterized by environmental and economic affordability and fairly high electrochemical performance [15]. The unique structure of perovskite materials allows improving the capacity of the material due to the vacancies in the cationic and anionic sublattices. The capacity of the material can be generated by changing the oxidation states of the transition metal. The LaMnO$_3$ compound of the stoichiometric composition contains only Mn^{3+} cations, and violation of stoichiometry leads to a change in the valence of some parts of manganese cations [16]. The conversion of Mn^{3+} to Mn^{4+} can be achieved by the presence of stoichiometric oxygen δ in undoped manganites LaMnO$_{3+\delta}$. In the nonstoichiometric compound, LaMnO$_{3+\delta}$ manganese is in three states Mn^{3+}, Mn^{2+}, Mn^{4+}. The oxygen index for manganites is in the range of 2.5 to 3.29 [17]. Excess oxygen (δ> 0) in the compound leads to an increase in the content of Mn^{4+} ions, and with oxygen deficiency (δ < 0) - anionic vacancies appear, and Mn^{3+} ions are oxidized to Mn^{2+}. Oxygen vacancy and the ability to ionic intercalation are important characteristics of the structure of perovskite material and significantly affect the specific capacity of LaMnO$_3$ nanoparticles [18]. The authors of [19] report that the electrochemical characteristics of LaMnO$_3$ material can be improved due to the porosity of the structure, which depends on the method of material synthesis. Mesopores and micropores in highly porous LaMnO$_3$ create channels for electrolyte diffusion. Accordingly, the rapid kinetics of charge transfer leads to an increase in electrochemical capacity. The electrochemical properties of perovskite material are dependent on the concentration and type of electrolyte ions. With the increasing concentration of electrolyte ions, there is an increase in oxygen vacancies, which in turn enhances the pseudocapacitor properties of materials with a perovskite structure [20]. Recently, many perovskite-carbon composites have appeared, such as LaMnO$_3$ / carbon [21], doped with LaNiO$_3$ / N-carbon [22], La$_{1-x}$Ca$_x$MnO$_3$ / graphene [23], RGO / LaAlO$_3$ [24], La$_2$NiO$_{4+\delta}$ @ Ag // AC [25], CaTiO$_3$ / activated carbon [26], which were obtained by various methods, including solid-phase synthesis, chemical deposition, sol-gel method, autoburning and others.

It is should be noted that carbon materials are considered the best materials for the EC. Moreover, carbon materials are inexpensive, easy to obtain, have high specific energy-intensive characteristics, chemically and electrochemically stable [27]. A significant improvement in the electrochemical parameters of such systems can be achieved due to combining carbon materials with other compounds, such as spinels [28] or manganese oxide [29]. Activated carbon (AC) is used as the active electrode material for supercapacitors due to its relatively low cost and high specific surface area of about 1000-2000 m^2/g [5, 30]. It is obtained from carbon-enriched organic precursors by carbonization (heat treatment) in an inert atmosphere followed by oxidation in CO$_2$, water vapor, or KOH to increase the specific surface area and pore volume. Natural or synthetic materials are used, such as coconut shells, wood resin, coal, or polymers, can be used as precursors. Activated carbon material with available micropores (< 2 nm),

mesopores (2 - 50 nm), and macropores (< 50 nm) was obtained by chemical activation. The wide pore size distribution is characteristic of the porous structure of carbon. Higher temperature or longer activation time leads to an increase in pore size [31].

Thus, by combining carbon materials with perovskite structures, it is possible to obtain hybrid electrode materials for supercapacitors, which are characterized by low cost, high values of electrical conductivity, and chemical stability. Therefore, to solve the problem of low specific energy, specific power, and service life of conventional supercapacitors, here we propose and characterize a new type of electrochemical system, and particularly a hybrid electrochemical capacitor based on the composite LaMnO$_3$ / activated carbon.

I. Methodology of the experiment

1.1 Synthesis of LaMnO₃

The complex LaMnO$_3$ oxide was synthesized by the sol-gel method with the participation of autoburning, the procedure of which is described in detail in [11]. Thus, 0.01 M lanthanum nitrate (La(NO$_3$)$_3$ · 6H$_2$O), 0.01 M manganese nitrate (Mn (NO$_3$)$_2$ · 6H$_2$O) and 0.02 M citric acid (C$_6$H$_8$O$_7$ · H$_2$O) were dissolved in deionized water and stirred on a magnetic stirrer. For establish the pH of 7 in the obtained solution was added a small amount of 25 % aqueous ammonia solution. The obtaining a solution was a milky pink color. A solution of dark burgundy color (purple) was obtained after continuous stirring of the solution for 4 hours.

The obtained sol was placed in a furnace at 400 K for 10 to 12 hours until the sol was completely dry. The polycondensation reaction with the formation of a gel has been performed during the dehydration process between citric acid and metal nitrates. Then the obtained material was heated to 570 K. After that, a few minutes later, the xerogels auto-burn process has been performed, as a result of which a free-flowing product LaMnO$_3$ was obtained.

The polarized electrode had been formed based on carbon material, which previously was experimentally obtained by carbonization and thermochemical activation with potassium hydroxide of raw materials of natural origin, the procedure of which is described in detail in [32].

1.2. Methods of investigation

The morphology of the obtained LaMnO$_3$ material was researched by field emission scanning electron microscope (SEM) JSM - 6700F. Secondary electron images were obtained on samples coated with the investigated of LaMnO$_3$ material under operating conditions of an accelerating voltage of 10 kV and a beam current of 0.75 nA.

The crystal structure of the sample was studied by X-ray diffraction (XRD) using a DRON 3.0 diffractometer with filtered Cu (Kα) radiation (λ = 1.5418 Å) in the range 15º- 70º. The results of the obtained diffractograms were performed by full-profile analysis by the Rietveld method using the program "FullProf" using the methodic described in [33]. From

the analysis of X-ray structural analysis data, the size of nanocrystallites of the studied sample and its phase composition were determined using methods described in [34].

Morphological characteristics of carbon material and LaMnO₃ manganite were determined using a NOVA Quantachrome 2200e gas sorption analyzer by analyzing nitrogen sorption isotherms at a temperature of T = 77 K. The essence of the research is to determine the volume of adsorbed (desorbed) nitrogen by the test sample at its boiling point and then calculate its morphological characteristics by various methods. The samples were pre-degassed in a vacuum chamber with a residual pressure of ~ 1.3 Pa at a temperature of 470 K for 18 hours. Moreover, the values of the specific surface area were determined using the BET method (S_{BET}) with a linear dependence of 1 / [W (p_0 / p) -1] on p_0 / p in the range of the adsorption isotherm for the ratio p_0 / p in the range from 0.05 to 0.35. In addition, Langmuir (S_L) and DFT (S_{DFT}) methods were used to determine the total surface area of LaMnO₃ perovskite material. Thus, the area of the micropores was determined by the t-method ($S_{t-micro}$), and the mesopores by the BJH method ($S_{BJH-meso}$). The total pore volume (V_{total}) was calculated from the amount of adsorbed nitrogen at P/P_0 ~ 1.0, the volume of micropores (V_{micro}) was determined using the t-method.

1.3. Electrochemical characteristics

A three-electrode cell was used to research the electrochemical behavior of the electrochemical systems of LaMnO₃/electrolyte and AC/electrolyte. The initial composition of the active material for the working electrode was a mixture of test material/acetylene black/ polyvinylidene fluoride (solution in ethanol) in a mass ratio of 85:10:5. On the next steps, the obtaining mixture was pressed into a nickel grid with a size of working electrode is 0.5 × 0.5 cm². Then, a sample was dried in an furnace at 350 K for 3 hours. The mass of the active material of LaMnO₃ and activated carbon, which in this case was 20 mg and 20 mg, respectively, was determined by weighing of the Ni-grid samples before and after forming the working electrode.

The additional electrode have been used a platinum electrode, the reference electrode was a chlorine-silver electrode (Ag/AgCl). The 3 M Li₂SO₄ was used as the electrolyte solution.

The electrochemical behaviors have been performed

using an Autolab PGSTAT / FRA-2 spectrometer in the frequency range from 10 MHz to 100 kHz. The specific capacitive parameters of LaMnO₃/electrolyte systems have been obtained using the cyclic voltammetry method. The specific capacitance of cyclic voltammetry (CVA) based on the integral area of the curves have been calculated using the equation (1) [35]:

$$C_m = \frac{C}{m} = \frac{\int_{V_2}^{V_1} IdV}{m \cdot \Delta V \cdot s}, \tag{1}$$

where C_m (F/g) is the specific capacitance, $\int_{V_2}^{V_1} IdV$ is the integral area of the CVA curve, I (mA) is the current, s (mV/s) is the scan rate, $\Delta V = V_2 - V_1$ is potential window (V), m (g) is a mass of active material.

To compare the results obtained, the specific capacity was measured by the galvanostatic method at operating currents from 1 mA to 8 mA. The measurements of the specific capacity C_m by Galvanostatic method of Charge / Discharge curve have been calculated using the equation (2) [36]:
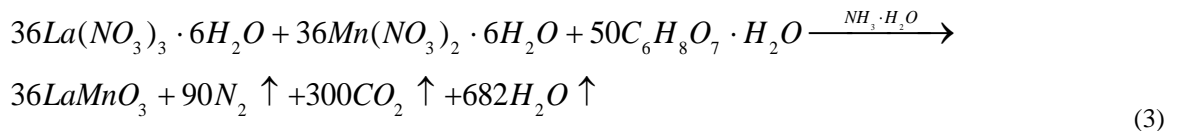
$$C_m = \frac{C}{m} = \frac{I \cdot \Delta t}{m \cdot \Delta V}, \tag{2}$$

where C_m (F/g) is the specific capacity, I (mA) is the charge-discharge current, Δt (s) is the discharge time, ΔV (V) is the potential during the discharge, m (g) is the mass of the active material.

The electrochemical behavior of the HEC$_S$ of LaMnO₃/electrolyte/AC system has been performed in a two-electrode cell. Furthermore, the HEC$_S$ electrodes have been formed based on the same technique. Finally, the electrodes have been separated by a separator and placed in an electrochemical cell, which was hermetically sealed after addition the solution of electrolyte.

II. Results and discussion

The compound LaMnO₃ is formed as a result of a chemical reaction:

$$36La(NO_3)_3 \cdot 6H_2O + 36Mn(NO_3)_2 \cdot 6H_2O + 50C_6H_8O_7 \cdot H_2O \xrightarrow{NH_3 \cdot H_2O}$$

$$36LaMnO_3 + 90N_2 \uparrow + 300CO_2 \uparrow + 682H_2O \uparrow \tag{3}$$

The technology and features of the synthesis of the investigated material are described in [37]. Figure 1a shows the diffraction patterns of the obtained material of LaMnO₃. According to data experimental X-ray diffraction pattern it was determined that the peak diffraction (2θ = 23, 32, 40, 46, 52, 58, 68) for the

obtained material is well indexed with the cubic phase of LaMnO₃. Thus, can be assuming that the obtained material has a perovskite structure of the spatial group Pm - 3m. It should be noted that LaMnO₃ with a perovskite structure can have both cubic (Pm - 3m) and rhombic (Pnma) lattices. Calculations have been carried
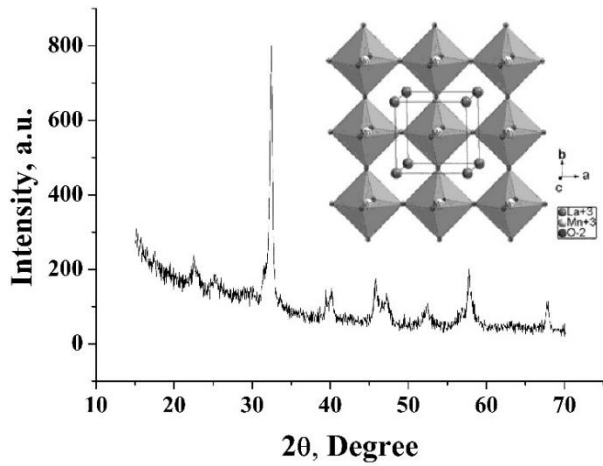
Fig. 1. The diffractograms of LaMnO$_3$ material, and model of LaMnO$_3$ crystal structure (view along the C axis) (insert).

out similarly to the methods described in [38-41] showed that LaMnO$_3$ with a perovskite structure forms exactly a cubic crystal lattice. Figure 1b shows a model of the crystal structure of the obtained material of LaMnO$_3$ (view along the C axis), which shows that the Mn cation is in an octahedral environment of O^{2-} anions. It was determined that the formed Mn-O bonds in the equatorial plane and axial vertices have a length of about 1.944 Å, and the length of O-O bonds through the axial vertices is about 2.7492 Å, according to the simulation data.

Moreover, La ions are located between equally oriented octahedral. The coordinate polyhedron has the shape of a cubic octahedron. The lattice constant of the synthesized material is a = 3.945 Å, and the volume is V = 61.38 Å^3. According to X-ray analysis, the density of the material is ρ = 6.54 g/cm^3. The average size of the coherent scattering regions is 24 nm.

Typical SEM images of the surface of the obtained material at various magnifications are shown in Fig. 2. It was found that the synthesized LaMnO$_3$ has a mesoporous structure with a particle size from 40 nm to 60 nm. The SEM images of high resolution show the clear crystallinity of the obtained material.
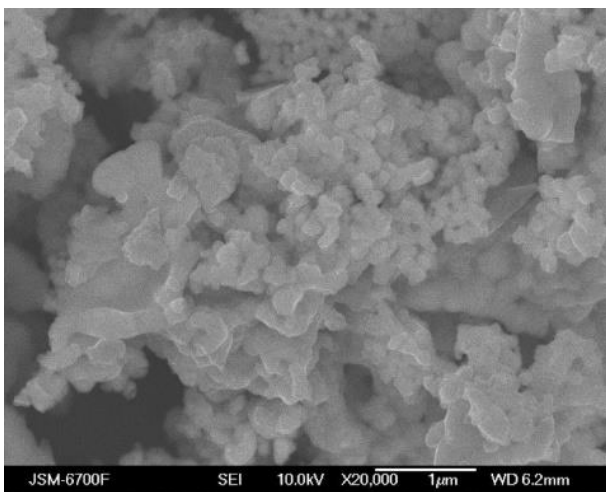

Fig. 2. SEM micrographs of LaMnO$_3$.

From adsorption-desorption isotherms of nitrogen by LaMnO$_3$ material was determined the pore size distribution by the DFT method Fig 3. The specific surface area of the obtained material is 42 m^2/g, was determined based on data of the BET method.

The pore size distribution according to the DFT method is presented in Fig. 3. The obtained material is mesoporous with a cavity size of 3 to 5 nm. It was determined that the mesoporous structure of the LaMnO$_3$ material is favorable for the diffusion of electrolyte ions.
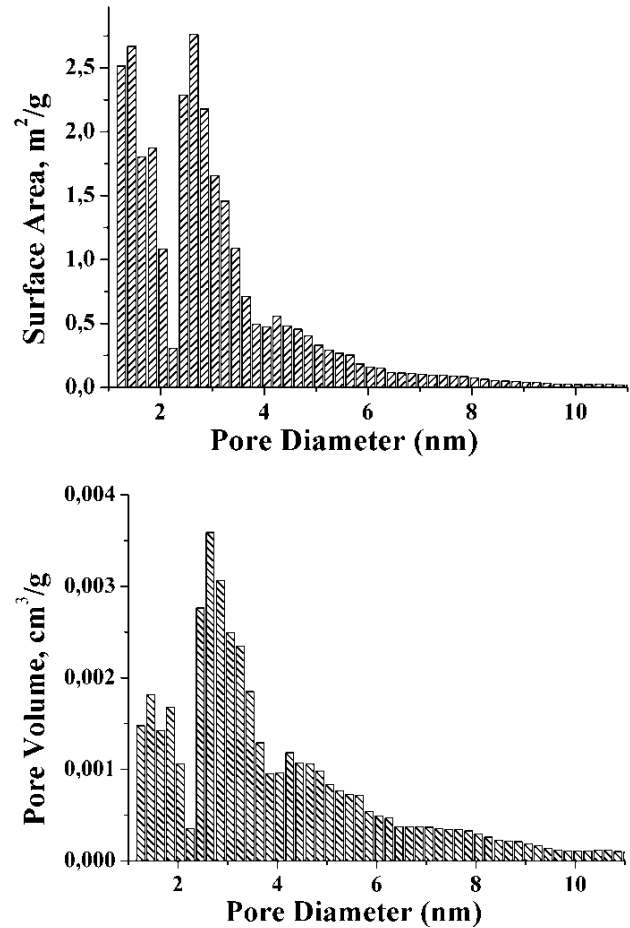

Fig. 3. Pore size distribution of the LaMnO$_3$.

Furthermore, assuming that the particles of the formed phase have a spherical shape, the average particle diameter d_c and the specific surface area S are related by the relation:

$$d_c = \frac{6}{\rho S},$$

(4)

where ρ is the density of the material. It was determined that the average particle size is 22 ± 2 nm based on X-ray density and the measured specific surface area by the BET method of the obtained material. Thus, on the one hand it can be assumed that the obtained material consists of particles with a size of 20 nm. On the other hand these particles are aggregated into particles with a size of 50 - 60 nm.
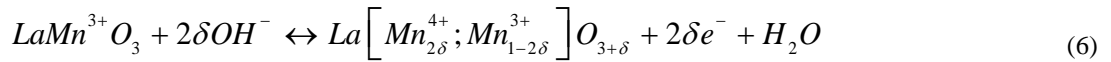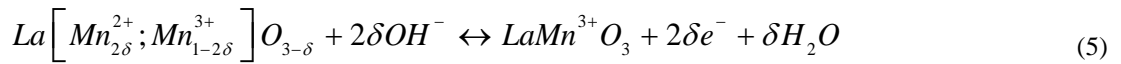
Quantitative characteristics of the porous structure of

the LaMnO$_3$ and AC are presented in Table 1.

The obtained activated carbon material is microporous with mesopores, accounting for up to 15 % of the total surface area. The surface area equal to 1236 m^2/g is determined by three methods correlated within an error of 10 %. The volume of micropores determined by the t-method is 0.41 cm^3/g, which is about 60% of the total pore volume determined at maximum pressure. Furthermore, the transport channels for the adsorbate or electrolyte into the micropores are due to by mesopores.

2.1. Electrochemical characteristics

The electrochemical behavior of the obtained LaMnO$_3$ material have been performed by cyclic voltammetry in the potential range from 0 V to 1 V relative to the Ag/AgCl reference electrode in the range of scan rate from 1 mV/s to 20 mV/s.

The CVA curves for the LaMnO$_3$/electrolyte system

at different scan rates are shown in Figure 4.a. CVA curves are asymmetric with the available redox peaks near 0.7 V and 0.5 V on the anode and cathode branches respectively, which shift with increasing scan rate toward lower potentials. The scan rate significantly affects the value of the specific capacitance of the electrodes. The dependence of the specific capacity of the obtained material LaMnO$_3$ on the scan rate is shown in Fig. 4.b. The maximum value of the specific capacity of the system LaMnO$_3$ / electrolyte is 35 F/g at a scan rate of 1 mV/s. Consequently, in materials with a perovskite structure, the accumulation and storage of charge occurs due to the diffusion of anions. The mechanism of anion diffusion and redox reactions for LaMnO$_3$ in the charge/discharge process can be represented by the equations of reactions (5) and (6) and Fig. 5 [42].

$$La\left[Mn_{2\delta}^{2+}; Mn_{1-2\delta}^{3+} \right]O_{3-\delta} + 2\delta OH^- \leftrightarrow LaMn^{3+}O_3 + 2\delta e^- + \delta H_2O \tag{5}$$

$$LaMn^{3+}O_3 + 2\delta OH^- \leftrightarrow La\left[Mn_{2\delta}^{4+}; Mn_{1-2\delta}^{3+} \right]O_{3+\delta} + 2\delta e^- + H_2O \tag{6}$$

During the oxidation process, at the first stage, oxygen-deficient $La\left[Mn_{2\delta}^{2+}; Mn_{1-2\delta}^{3+} \right]O_{3-\delta}$ absorbs OH group ions from the electrolyte, which is based on O^{2-} and H$_2$O.

As a result, O^{-2} ions diffuse along the octahedral oxygen faces in the perovskite lattice and occupy oxygen vacancies in the bulk structure of the material. Thus, in the perovskite structure there is a transition Mn^{2+} to

Mn^{3+}, forming a definitively neutral La Mn^{3+}O$_3$. Finally in the next stage, manganese ions deviate from the center of the oxygen octahedron, and the excess oxygen diffuses on the surface, as a result of which the ions Mn^{3+} are oxidized to Mn^{4+}, forming an excess of oxygen $La\left[Mn_{2\delta}^{4+}; Mn_{1-2\delta}^{3+} \right]O_{3+\delta}$ [42].

Figure 4.b shows that with an increase in scan rate, the capacity of the material decreases. The total capacity

Table 1

Sorption characteristics of AC and LaMnO$_3$

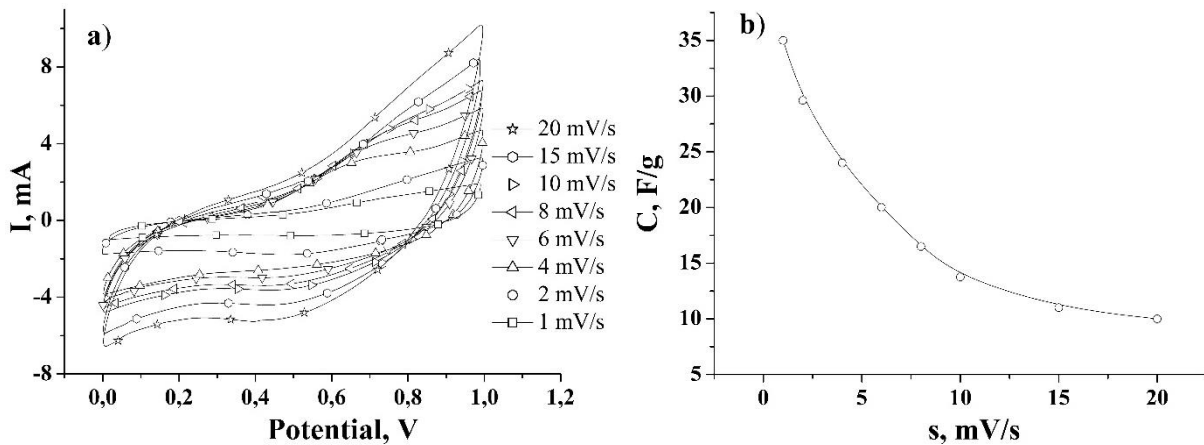| Sample	S_{BET}, m^2/g	S_L, m^2/g	S_{DFT}, m^2/g	$S_{t\text{-micro}}$, m^2/g	$S_{BJH\text{-meso}}$, m^2/g	S_{micro}, %	V_{total}, cm^3/g	V_{micro}, cm^3/g
AC	1236	1405	1085	1040	160	84	0,69	0,41
LaMnO$_3$	42	44	28	12	20	28	0.05	0.01

Fig. 4. Potentiodynamic curves obtained for the LaMnO$_3$ / electrolyte system at scan rate from 1 mV/s to 20 mV/s a) and the dependence of the specific capacity of the system on the scan rate b).

of the researched material can be divided into the capacity of the double electric layer (C$_{DEL}$) and diffusion-controlled redox capacity due to Faraday reversible redox reactions (C$_F$): $C = C_{DEL} + C_F$ [43]. In the kinetic model [43], it is assumed that the scan rate affects the total specific electrochemical capacity of the system, because the diffusion component of the capacity (C$_F$) is a function of the reaction time. Therefore, the scan rate can be considered inverse to the time of diffusion. Thus, in the case of semi-infinite linear diffusion, the total capacity is related to the scan rate by the following equation:

$$C = C_{s=\infty} + a\frac{1}{\sqrt{s}}$$, where a is a constant value, and

$C_{DEL} = C_{s=\infty}$. As follows from Fig. 6 a, the specific capacity of the material LaMnO$_3$ linearly depends on $s^{-1/2}$. Extrapolation of the dependences C from $s^{-1/2}$ to the Y axis (Fig. 6,a) made it possible to determine the redox capacity due to Faraday reversible redox reactions and the DEL capacity of the investigated materials (Table 2).

The dependence of the specific capacitance of the LaMnO$_3$/electrolyte system on the scan rate can also be extrapolated to the other side to s = 0, using the functional dependence on s. Since C increases linearly with $s^{-1/2}$, then 1/C shut decrease linearly with $s^{1/2}$. Then,

$$\frac{1}{C} = \frac{1}{C_{s=0}} + b\sqrt{s}$$ where $C_{s=0}$ is the maximum specific

capacity that can be obtained, b is a constant value (Fig. 6,b). Figure 6,b shows the value inverse to the specific capacity linearly depends on $s^{1/2}$. Moreover, extrapolation of C^{-1} dependences from $s^{1/2}$ to the Y axis (6.b) made it possible to determine the maximum specific
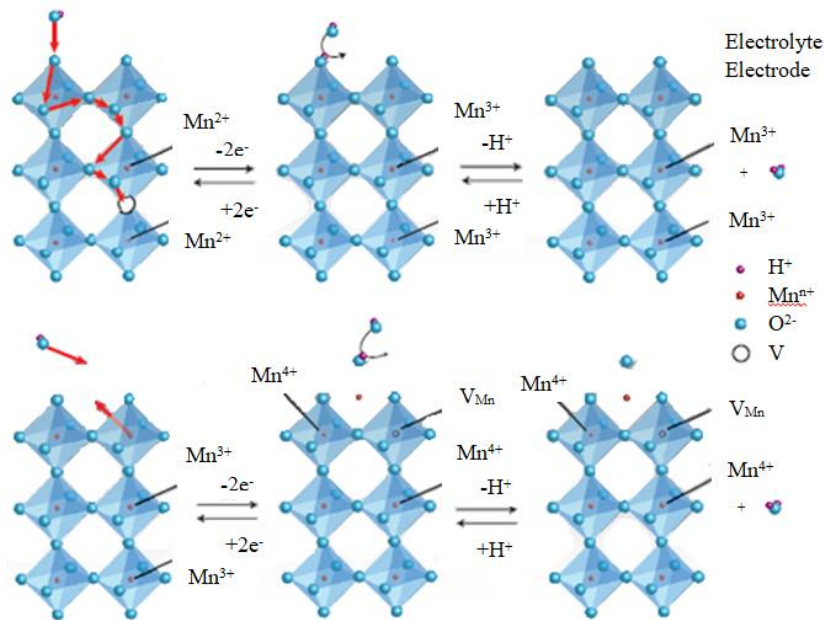
Fig. 5. The mechanism of diffusion of OH groups in LaMnO$_{3 \pm \delta}$.
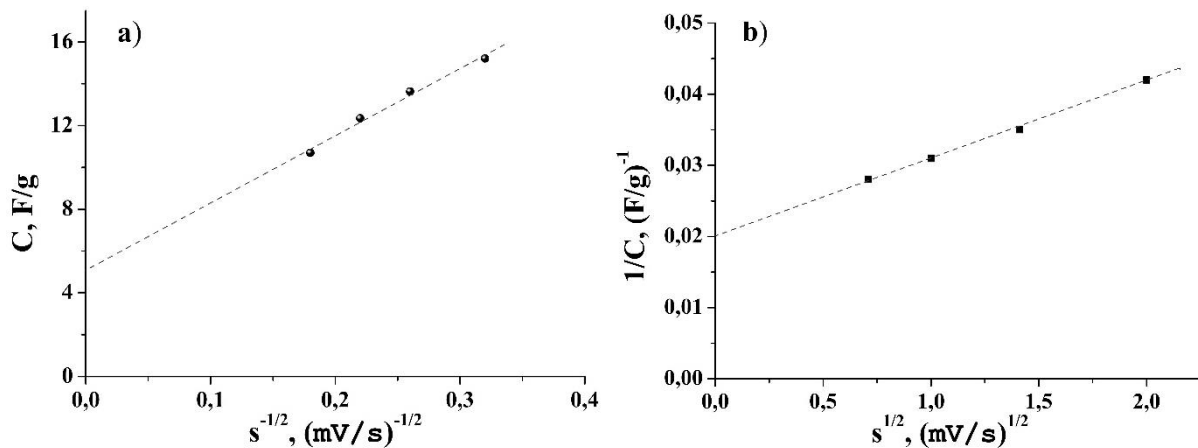
Fig. 6. Dependence of the specific capacity of the LaMnO$_3$/electrolyte system on $s^{1/2}$ a) and 1/C on $s^{1/2}$ b).
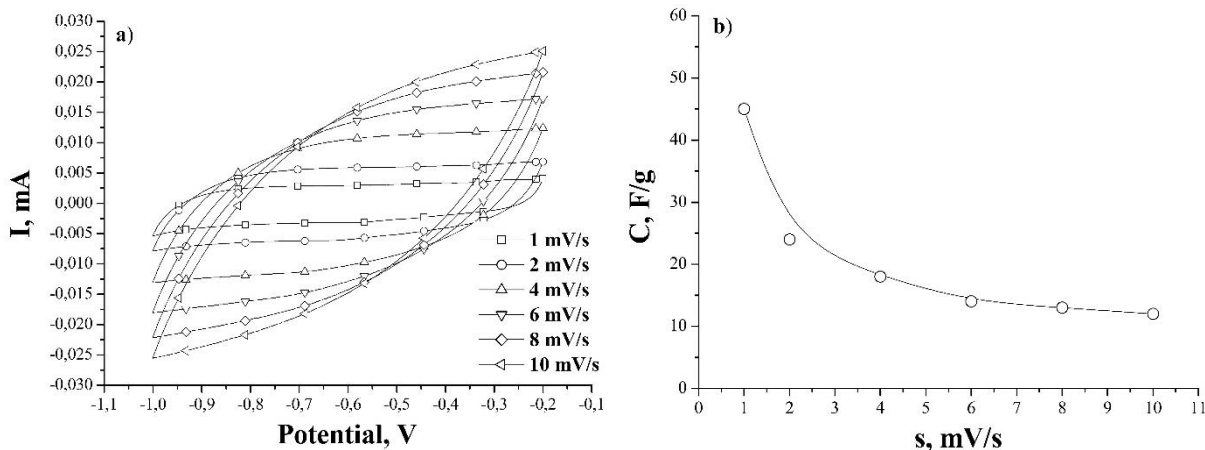
Fig. 7. Potentiodynamic curves obtained for the system AC/electrolyte a) and the dependence of the specific capacity of the system on the scan rate b).

capacity of the researched system of LaMnO₃/electrolyte (Table 2).

The CVA curves of the AC/electrolyte system are typical for EC with DEL (Fig. 7,a). As the scan rate increases from 1 mV/s to 10 mV/s, the potentiodynamic curves deviate from the rectangular shape due to the increase in the internal resistance of the system.

The shape of the obtained CVA curves is typical for EC with carbon electrodes in aqueous electrolytes [32]. At low CVA scan rates, the curves have a symmetrical close to rectangular shape and, typically, there are no peaks that are responsible for the course of redox processes in this system. The maximum value of the specific capacity (Fig. 7,b) of the carbon electrode in the Li_2SO_4 electrolyte is 45 F/g. Figure 7,b shows that the value of the specific capacity of the system AC/electrolyte decreases monotonically with increasing of scan rate. It shut be noted that the change in specific capacity from the scan rate for both systems is almost the same, which is positive in the operation of these systems in co-operation.

Based on of the electrochemical behavior of carbon material and perovskite material LaMnO₃ in the negative potential and in the positive region, a hybrid electrochemical system type AC / Li_2SO_4 / LaMnO₃ was formed. Thus, the use in the electrochemical system of materials with different nature of charge accumulation allows it to function at higher voltages, and, accordingly, increases the energy performance of the electrochemical characteristics of system. The research of the joint functioning of electrode materials in a hybrid electrochemical system was carried out by the potentiodynamic method. The optimal operating voltage of a single element has been determine, potentiodynamic investigations were performed with a gradual increase in the maximum voltage in steps of 0.2 V in the range from 0 V to 2 V (Fig. 8).

The operation of the electrochemical system was stable in the whole voltage range, so further electrochemical investigations were performed in this potential range.

All CVA curves (Fig. 9,a) are characterized by the presence of redox peaks, which are responsible for the redox reactions, mainly according to the scheme:
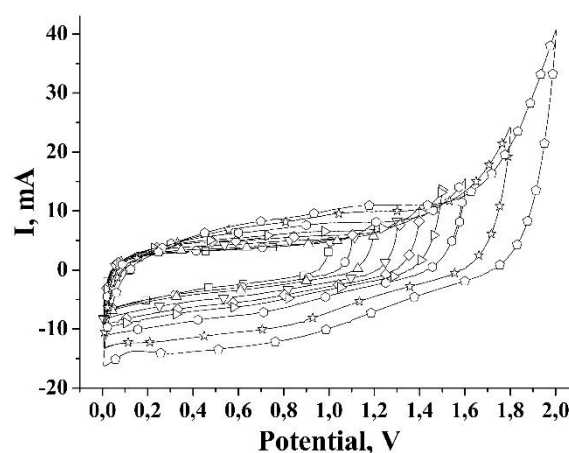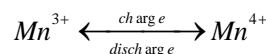

Fig. 8. Potentiodynamic curves of the AC / Li_2SO_4 / LaMnO₃ system at a scan rate of 1 mV/s.

$$Mn^{3+} \underset{disch\arg e}{\overset{ch\arg e}{\longleftrightarrow}} Mn^{4+}$$

Based on the experimentally obtained potentiodynamic curves (Fig. 9, a) the dependence of the specific capacity of the HEC of the AC/Li₂SO₄/LaMnO₃ system on the scan rate was determined (Fig. 9, b). The maximum value of the specific capacity is 53 F/g at a scan rate of 1 mV/s. The HEC model showed stability in the voltage range from 0 V to 2 V for more than 500 cycles.

The discharge curves of the investigated electrochemical systems are shown in Fig. 10. The discharge curves for the LaMnO₃/electrolyte system in the positive potential range (Fig. 10, a) are characterized by two linear sections with different slope angles, which indicates two different mechanisms of accumulation of electrical energy. The charge-discharge curve for the LaMnO₃/electrolyte system shows that the discharge time decreases with increasing current. This probably due to the fact that at high discharge currents there is not enough time for the electrolyte ions to fully penetrate into the electrode materials and enter the vacancy. Consequently, there is a linear dependence of the voltage on time, at a constant current, which indicates an

650

electrostatic accumulation of charge for the AC/electrolyte electrochemical system in the negative potential range (Fig. 10, b).

The use of materials with different nature of charge accumulation and in different potential ranges made it possible to design a hybrid electrochemical system operating at a maximum voltage of 2 V in an aqueous electrolyte (Fig. 11, a).

At low operating currents on the discharge curves (Fig. 11, a), there is practically no voltage drop during discharge, which indicates the minimum internal resistance of the designed electrochemical system. The system under investigation is electrochemically stable in this voltage range, as evidenced by the constant value of
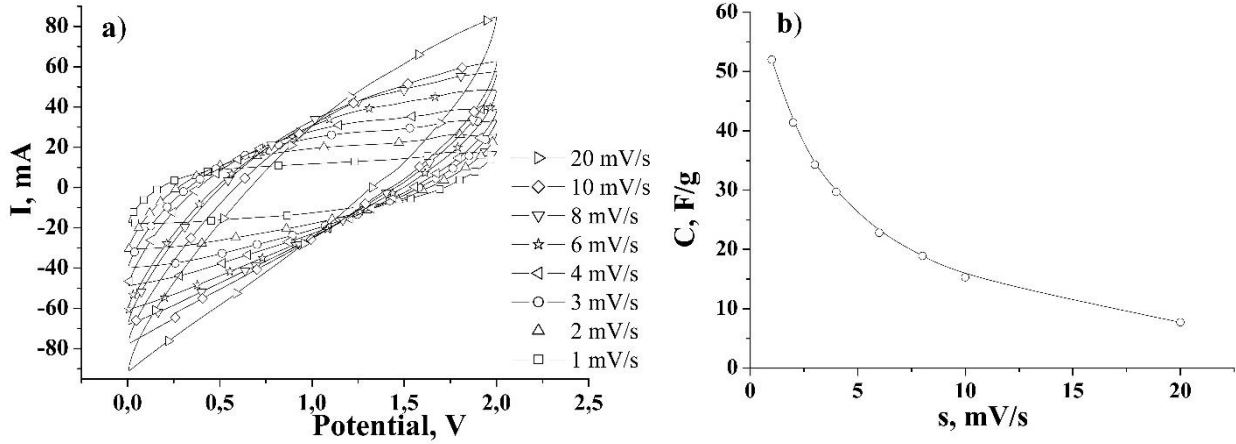

Fig. 9. Potentiodynamic curves of AC/Li$_2$SO$_4$/LaMnO$_3$ systems in the voltage range from 0V to 2V at scan rate of from 1 mV/s to 20 mV/s a) and the dependence of the specific capacity of the system on the scan rate b).
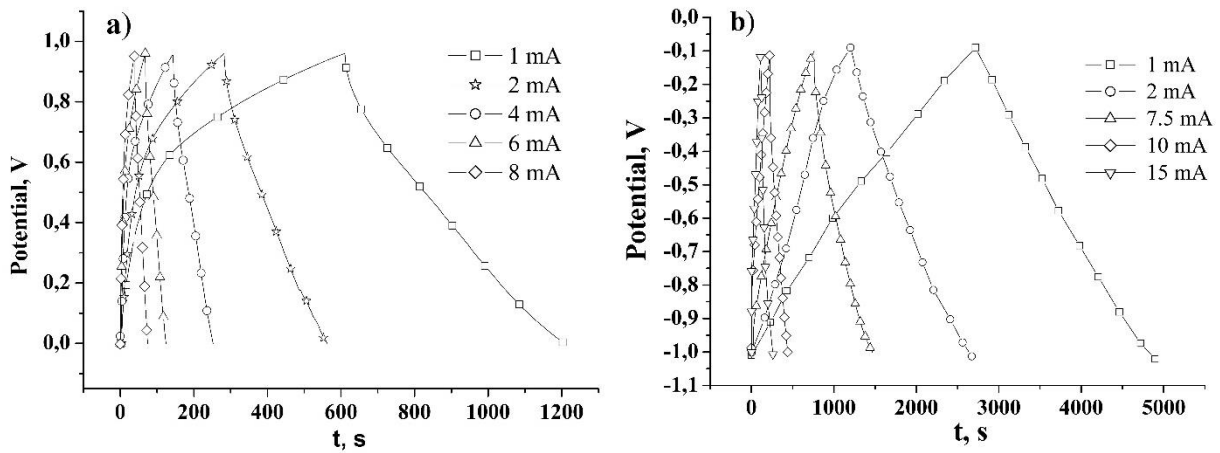

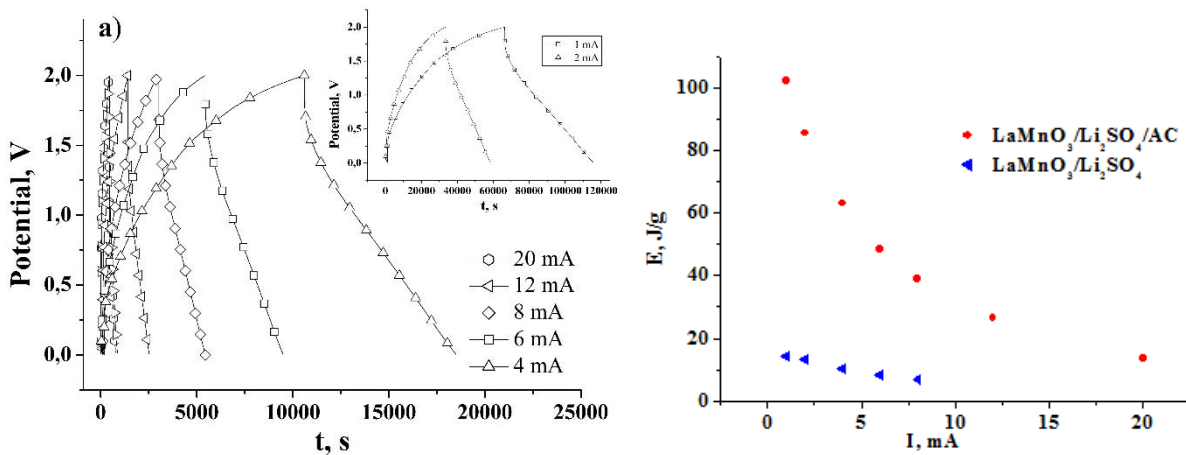**Fig. 10.** Charge-discharge curves for the LaMnO$_3$/Li$_2$SO$_4$ a) and AC/Li$_2$SO$_4$ systems b) at different currents.

Fig. 11. Charge / discharge curves of HEC AC / Li$_2$SO$_4$ / LaMnO$_3$ a) and the dependence of the specific energy on the discharge current b).

the Coulomb efficiency over more than 500 operating cycles. Therefore, based on the obtained discharge curves (Fig. 10 and Fig. 11,a), the specific energy characteristics of the systems under research were determined (Fig. 11,b), namely, the dependence of the specific energy on the discharge current. Finally, the maximum values of the specific energy for the systems $LaMnO_3$/electrolyte, AC/electrolyte, and HEC with electrodes based on $AC/Li_2SO_4/LaMnO_3$ are 14.3, 73.9, and 112.1 J/g, respectively.

Conclusions

Analyzing the X-ray diffraction and electron microscopy data, it was determined that the investigated $LaMnO_3$ material has a perovskite structure with particle sizes of 22 ± 2 nm and from 40 nm to 60 nm respectively.

The investigation of the electrochemical behavior for the $LaMnO_3/Li_2SO_4$ system has been performed. Moreover, the specific capacity of the investigated material has been determined, which in this case is 35 F/g at a scan rate of 1 mV/s.

The total capacitance of the electrochemical system $LaMnO_3/Li_2SO_4$ is divided into a capacitance the accumulation of charge in the double electric layer and a diffusion-controlled redox capacitance due to fast Faraday reversible redox reactions. It is determined that the main contribution to the total capacity is made by the Faraday capacity, which is ~ 90 % of the total capacity. The electrochemical processes occurring in the AC/Li_2SO_4 system are described, and it is shown that the obtained CVA curves are typical for EC with DEL. The maximum value of the specific capacity of this system is 45 F/g.

A hybrid electrochemical capacitor based on $LaMnO_3$, as the active material of the Faraday electrode, in combination with a polarized electrode based on carbon material obtained from raw materials of organic origin and its main energy parameters were determined in a potential range of 0 - 2 V. Moreover, it is shown that the electrochemical system based on an aqueous electrolyte of 3 M Li_2SO_4 is stable in the operating voltage range $0 - 2$ V and has a maximum value of specific capacity of 53 F/g.

It was determined that the maximum values of specific energy for $LaMnO_3$ / electrolyte, AC / electrolyte, and HEC systems with electrodes based on AC / Li_2SO_4 / $LaMnO_3$ are 14.3, 73.9, and 112.1 J/g, respectively.

Kolkovska H.M. – PhD student of Material Science and New Technology Department;
Rachiy B.I. – Dr. Phys.-Math. Sci., Prof. of Material Science and New Technology Department, д.ф.-м.н.;
Kolkovskyi P.I. – PhD, post-doc of Material Science and New Technology Department;
Yaremiy I.P. – Dr. Phys.-Math. Sci., Prof. of Material Science and New Technology Department;
Ivanichok N.Ya - PhD, senior researcher of Material Science and New Technology Department;
Lisovskiy R.V., – Dr. Phys.-Math. Sci., Prof. of Medical Informatics and Medical and Biological Physics;
Ilnytskyi N.R. – student*.*

[1] F. Wang, X. Wu, X. Yuan, Z. Liu, Y. Zhang, L. Fu, Y. Zhu, Q. Zhou, Y. Wu, W. Huang, Chemical Society Reviews 6(22), 6816 (2017); https://doi.org/10.1039/c7cs00205j.
[2] V. Boychuk, V. Kotsyubynsky, B. Rachiy, K. Bandura, A. Hrubiak, S. Fedorchenko, Materials Today: Proceedings 6(2), 106 (2019); https://doi.org/10.1016/j.matpr.2018.10.082.
[3] M. Salanne, B. Rotenberg, K. Naoi, K. Kaneko, P.L. Taberna, C. P. Grey, B. Dunn, P. Simon, Nature Energy 1, 16017 (2016); https://doi.org/10.1038/nenergy.2016.70.
[4] R.Y. Shvets, I.I. Grygorchak, A.K. Borysyuk, S.G. Shvachko, A.I. Kondyr, V.I. Baluk, A.S. Kurepa, B.I. Rachiy, Physics of the Solid State 56(10), 2021 (2014); https://doi.org/10.1134/S1063783414100266.
[5] L.L. Zhang, X.S. Zhao, Chemical Society Reviews 38(9), 2520 (2009); https://doi.org/10.1039/B813846J.
[6] E. Arendt, A. Maione, A. Klisinska, O. Sanz, M. Montes, S. Suarez, J. Blanco, P. Ruiz, Applied Catalysis A: General 339(1), 1 (2008); https://doi.org/10.1016/j.apcata.2008.01.016.
[7] Y. Tokura, Colossal Magnetoresistive Oxides (Amsterdam, Gordon and Breach Science and Publishers, 2000).
[8] D. Munoz, N.M. Harrison, F. Illas, Physical Review B 69, 8 (2004); https://doi.org/10.1103/PhysRevB.69.085115.
[9] S.A. Veldhuis, P.P. Boix, N. Yantara , M. Li, T.C. Sum, N. Mathews, S.G. Mhaisalkar, Advansed Materials 28(32), 6804 (2016); https://doi.org/10.1002/adma.201600669.
[10] N.G. Park, Materials today 18(2), 65 (2015); https://doi.org/10.1016/j.mattod.2014.07.007.
[11] Y. Li, S. Yao, L. Xue, Y. Yan, Journal of Materials Science 44(16), 4455 (2009); https://doi.org/10.1007/s10853-009-3673-7.
[12] C. Jin, X. Cao, L. Zhang, C. Zhang, R. Yang, J. Power Sources 241, 225 (2013); doi:org/10.1016/j.jpowsour.2013.04.116.
[13] J. Hu, L. Shi, Q. Liu, H. Huang, T. Jiao, RSC Advances 5, 92096 (2015); https://doi.org/10.1039/c5ra14928b.

[14] P.P. Ma, Q.L. Lu, N. Lei, Y.K. Liu, B. Yu, J.M. Dai, S.H. Li, G.H. Jiang, Electrochimica Acta 332, 135489 (2020); https://doi.org/10.1016/j.electacta.2019.135489.

[15] H. Nan, X. Hu, H. Tian, Materials Science in Semiconductor Processing 94, 35 (2019); https://doi.org/10.1016/j.mssp.2019.01.033.

[16] E.L. Nagaev, Uspekhi Phys. Nauk 166(8), 833 (1996) doi: 10.3367/UFNr.0166.199608b.0833 .

[17] A.O. Novokhatska, Influence of excess manganese on the formation of the structure and magnetoresistive properties of doped manganites (Kyiv, 2018).

[18] Z.A. Elsiddig, H. Xu, D. Wang, W. Zhang, X. Guo, Y. Zhang, Z. Sun, J. Chen, Electrochimica Acta 253, 422 (2017).

[19] P Muhammed Shafi, A Chandra Boseand, Ajayan Vinu, Chem. Electro Chem. 5(23), 3723 (2018); https://doi.org/10.1002/celc.201801053.

[20] K.C. Tsay, L. Zhang, J. Zhang, Electrochimica Acta 60, 428 (2012); https://doi.org/10.1016/j.electacta.2011.11.087.

[21] J. Liu, X. Jin, W. Song, F. Wang, N. Wang, Y. Song, Chinese Journal of Catalysis 35(7), 1173 (2014); https://doi.org/10.1016/S1872-2067(14)60066-8.

[22] W.G. Hardin, D.A. Slanac, X. Wang, S. Dai, K.P. Johnston, K.J. Stevenson, The Journal of Physical and Chemistry Letters 4(8), 1254 (2013); https://doi.org/10.1021/jz400595z.

[23] J. Hu, L. Wang, L. Shi, H. Huang, Journal of Power Sources 269, 144 (2014); https://doi.org/10.1016/j.jpowsour.2014.07.004.

[24] T.N. Vinuth Raj, Priya A. Hoskeri, H.B. Muralidhara, C.R. Manjunatha, K. Yogesh Kumar, M.S. Raghu, Journal of Electroanalytical Chemistry 858, 113830 (2020); https://doi.org/10.1016/j.jelechem.2020.113830.

[25] Mingrui Wei, Wei Chea, Haizhao Li, Zhihao Wang, Fuwu Yan, Yihui Liu, Applied Surface Science 484, 551 (2019); https://doi.org/10.1016/j.apsusc.2019.04.015.

[26] X.-Li Cao, T-Zh Ren, Z-Y Yuan, T. J. Bandosz, Electrochimica Acta 268, 73 (2018); https://doi.org/10.1016/j.electacta.2018.02.069.

[27] B.I. Rachiy, I.M. Budzulyak, V.M. Vashchynsky, N.Y. Ivanichok, M.O. Nykoliuk, Nanoscale Research Letters 11(1), 18 (2016); https://doi.org/10.1186/s11671-016-1241-z.

[28] T.Y. Boychuk, I.M. Budzulyak, N.Y. Ivanichok, R.P. Lisovskiy, B.I. Rachiy, Journal of Nano- and Electronic Physics 7(1), 01019 (2015).

[29] B.K. Ostafiychuk, I.M. Budzulyak, B.I. Rachiy, R.P. Lisovsky, V.I. Mandzyuk, P.I. Kolkovsky, R.I. Merena, M.V. Berkeshchuk, L.V. Golovko, Journal of Nano- and Electronic Physics 9(5), 05001 (2017); https://doi.org/10.21272/jnep.9(5).05001.

[30] Ahmed Afif, Sheikh MH Rahman, Atia Tasfiah Azad, Juliana Zaini, Md Aminul Islan, Abul Kalam Azad, Journal of Energy Storage 25, 100852 (2019); https://doi.org/10.1016/j.est.2019.100852.

[31] B.K. Ostafiychuk, R.P. Lisovskiy, A.-S.A.H. Zamil, V.O. Kotsyubynsky, P.I. Kolkovsky, R.I. Merena, A.B. Hrubiak, Journal of Nano- and Electronic Physics 11(3), 03036 (2019); https://doi.org/10.21272/jnep.11(3).03036.

[32] B.K. Ostafiychuk, I.M. Budzulyak, B.I. Rachiy, V.M. Vashchynsky, V.I. Mandzyuk, R.P. Lisovsky, L.O. Shyyko, Nanoscale Research Letters 10(1), 65 (2015); https://doi.org/10.1186/s11671-015-0762-1.

[33] I. Yaremiy, S. Yaremiy, V. Fedoriv, O. Vlasii, A. Lucas, Eastern-European Journal of Enterprise Technologies 5(5(95)), 61 (2018); https://doi.org/10.15587/1729-4061.2018.142752.

[34] V.S. Bushkova, S.I. Mudry, I.P. Yaremiy, V.I. Kravets, Journal of Physical Studies 20(1/2), 1702 (2016); https://doi.org/10.30970/jps.20.1702.

[35] K. Krishnamoorthy, G.K. Veerasubramani, S. Radhakrishnan, S.J. Kim, Chemical Engeneering Journal 251, 116 (2014); https://doi.org/10.1016/j.cej.2014.04.006.

[36] A. Wang, H. Wang, S. Zhang, C. Mao, J. Song, H. Niu, B. Jin, Y. Tian, Applied Surface Science 282, 704 (2013); https://doi.org/10.1016/j.apsusc.2013.06.038.

[37] Y. Li, L. Xue, L. Fan, Y. Yan, Journal of Alloys and Compounds 478(1-2), 493 (2009); https://doi.org/10.1016/j.jallcom.2008.11.068.

[38] D. Freik, T. Parashchuk, B. Volochanska, Journal of Crystal Growth 402, 90 (2014); https://doi.org/10.1016/j.jcrysgro.2014.05.005.

[39] R. Ahiska, D. Freik, T. Parashchuk, I. Gorichok, Turkish Journal of Physics 38(1), 125 (2014).

[40] I.V. Horichok, L.I. Nykyruy, T.O. Parashchuk, S.D. Bardashevska and M.P. Pylyponuk, Modern Physics Letter B 30(16), 1650172 (2016); https://doi.org/10.1142/S0217984916501724.

[41] O. Cherniushok, R. Cardoso-Gil, T. Parashchuk, Y. Grin, K.T. Wojciechowski, Inorganic Chemistry 60(4), 2771 (2021); https://doi.org/10.1021/acs.inorgchem.0c03549.

[42] J.T. Mefford, W.G. Hardin, S. Dai, K.P. Johnston, K.J. Stevenson, Nature Materials 13(7), 726 (2014); https://doi.org/10.1038/nmat4000.

[43] M.W. Xu, L.B. Kong, W.J. Zhou, H.L. Li, Journal of Physical Chemistry C 111(51), 19141 (2007); https://doi.org/10.1021/jp076730b.

H.M. Kolkovska, B.I. Rachiy, P.I. Kolkovskyi, I.P. Yaremiy, N.Ya. Ivanichok, R.P. Lisovskiy, N.R. Ilnytskyi

Г.М. Колковська[1], Б.І. Рачій[1], П.І. Колковський[1], І.П. Яремій[1],
Н.Я. Іванічок[1], Р.П.Лісовський[2], Н.Р. Ільницький[2]

Механізми накопичення заряду електрохімічної системи LaMnO₃ / AC

[1]Прикарпатський національний університет імені Василя Стефаника, Івано-Франківськ, Україна,
Pkolkovskyy@gmail.com
[2]Івано-Франківський національний медичний університет, Івано-Франківськ, Україна, Rlisovsky@ifnmu.edu.ua

У роботі досліджується електрохімічна поведінка перовскітового матеріалу $LaMnO_3$ та нанопористого вуглецевого матеріалу у водному розчині сульфату літію. Визначено закономірності доцільності спільного функціонування цих матеріалів як електродів для гібридного електрохімічного конденсатора. Встановлено, що значення питомої ємності досліджуваної електрохімічної системи $LaMnO_3$ / електроліт / змінне середовище становить 52 Ф/г під час розряду системи до 1 В, а питома енергія - 112,1 Дж / г при струмі розряду 1 мА.

Ключові слова: манганіт $LaMnO_3$, активоване вугілля, електроліт Li_2SO_4, питома ємність.